

# Highly efficient room-temperature nonvolatile magnetic switching by current in $\text{Fe}_3\text{GaTe}_2$ thin flakes

Shaohua Yan,<sup>†,‡,||</sup> Shangjie Tian,<sup>¶,‡,||</sup> Yang Fu,<sup>†,‡</sup> Fanyu Meng,<sup>†,‡</sup> Zhiteng Li,<sup>§</sup>  
Shouguo Wang,<sup>\*,¶</sup> Xiao Zhang,<sup>\*,§</sup> and Hechang Lei<sup>\*,†,‡</sup>

<sup>†</sup>*Department of Physics and Beijing Key Laboratory of Optoelectronic Functional Materials & MicroNano Devices, Renmin University of China, Beijing 100872, China*

<sup>‡</sup>*Key Laboratory of Quantum State Construction and Manipulation (Ministry of Education), Renmin University of China, Beijing, 100872, China*

<sup>¶</sup>*School of Materials Science and Engineering, Anhui University, Hefei 230601, China*

<sup>§</sup>*State Key Laboratory of Information Photonics and Optical Communications & School of Science, Beijing University of Posts and Telecommunications, Beijing 100876, China*

*|| These authors contributed equally to this work.*

E-mail: sgwang@ahu.edu.cn; zhangxiaobupt@bupt.edu.cn; hlei@ruc.edu.cn

## Abstract

Effectively tuning magnetic state by using current is essential for novel spintronic devices. Magnetic van der Waals (vdW) materials have shown superior properties for the applications of magnetic information storage based on the efficient spin torque effect. However, for most of known vdW ferromagnets, the ferromagnetic transition temperatures lower than room temperature strongly impede their applications and the room-temperature vdW spintronic device with low energy consumption is still a

long-sought goal. Here, we realize the highly efficient room-temperature nonvolatile magnetic switching by current in a single-material device based on vdW ferromagnet  $\text{Fe}_3\text{GaTe}_2$ . Moreover, the switching current density and power dissipation are about 300 and 60000 times smaller than conventional spin-orbit-torque devices of magnet/heavy-metal heterostructures. These findings make an important progress on the applications of magnetic vdW materials in the fields of spintronics and magnetic information storage.

**keywords:**nonvolatile magnetic switching,room-temperature, highly efficient, van der Waals crystals

## Introduction

Two-dimensional magnetic materials are new members of the two-dimensional material family. They still maintain long-range magnetic order at the thickness of a single unit cell and are easily controlled by external fields.<sup>1-7</sup> This provides an ideal platform for the study of magnetism and other novel physical effects under two-dimensional limits. Moreover, owing to their intrinsic two-dimensional (2D) long-range magnetism and the easiness of combination with other van der Waals (vdW) materials, the vdW 2D magnets also exhibit significant advantages in the design and preparation of multi-functional vdW devices with reduced size of device, especially spintronic devices.<sup>8-10</sup> Thus they have been attracted intensive attention. Among the known vdW magnetic materials, the Fe-based systems, such as  $\text{Fe}_x\text{GeTe}_2$  ( $x = 3, 4, 5$ ) and  $\text{Fe}_3\text{GaTe}_2$ , exhibit superior properties like high magnetic transition temperature ( $T_c$ ) up to about 380 K and large coercivity of approximately several kOe at low temperature with the  $c$  axis magnetic anisotropy.<sup>4,11-13</sup> More importantly, such features of hard magnetism with high  $T_c$  persist in the atomically thin samples and can be tuned via various methods, such as doping, pressure, gating etc.<sup>3,4,14</sup>

Effective control of magnetic state by using current is at the core of spintronics field.<sup>15,16</sup> The

adjustable coercivity by current makes it possible to simultaneously achieve high efficiency and nonvolatile characteristics in devices. For an information writing process, the coercive field ( $H_c$ ) need be reduced to relatively low value and the information can be written with low energy consumption. On the other hand, once the information has been written, the  $H_c$  should be big enough to reduce the information loss caused by fluctuations. Previous studies demonstrate that the nonvolatile and energy-efficient magnetization switching by current can be achieved in single vdW ferromagnet  $\text{Fe}_3\text{GeTe}_2$ .<sup>17,18</sup> But the  $T_c$  of  $\text{Fe}_3\text{GeTe}_2$  lower than room temperature limits its application. In contrast, the  $c$ -axial vdW hard ferromagnet  $\text{Fe}_3\text{GaTe}_2$  has a much higher  $T_c$  than 300 K. Moreover, based on  $\text{Fe}_3\text{GaTe}_2$  thin flakes, some room-temperature magnetic tunneling junction and spin-orbit torque (SOT) devices have been reported.<sup>19–22</sup>

Motivated by the studies of current-controlled magnetic switching in  $\text{Fe}_3\text{GeTe}_2$  and the superior properties of  $\text{Fe}_3\text{GaTe}_2$ , in this work, we study the evolution of coercive field  $H_c$  with the  $ab$ -plane current for  $\text{Fe}_3\text{GaTe}_2$  thin flakes. The  $H_c$  can be reduced remarkably using the relatively low current density and importantly the current-controlled  $H_c$  still exists at room temperature. Furthermore, the nonvolatile magnetic switching by current is realized at room-temperature with high efficiency. Switching current density and power dissipation at 300 K are about 300 and 60000 times smaller than conventional ferromagnet/heavy-metal systems, Such a high-efficiency room-temperature magnetic memory device could be a key component in the area of all-vdW spintronics.

## Results and discussion

The  $\text{Fe}_3\text{GaTe}_2$  thin flakes were exfoliated from high-quality bulk crystals grown by self-flux method. As is shown in Fig. 1a,  $\text{Fe}_3\text{GaTe}_2$  has a layered structure with a hexagonal structure (space group  $P6_3/mmc$ ),<sup>4</sup> isostructural to  $\text{Fe}_3\text{GeTe}_2$ , and the fitted lattice parameters  $a$  and

$c$  from the single-crystal X-ray diffraction (XRD) pattern is 0.409(2) nm and 1.607(2) nm, respectively, which are consistent with previous results.<sup>4</sup> In the Fe-Ga-Te layer, the Fe-Ga slab is sandwiched by the Te atoms and there is a vdW gap between two adjacent Fe-Ga-Te slabs, thus it can be exfoliated easily. Fig. 1b shows the XRD pattern of a Fe<sub>3</sub>GaTe<sub>2</sub> single crystal and only sharp (00 $l$ ) diffraction peaks are observable, indicating that the crystal surface is normal to the  $c$ -axis with the plate-shaped surface parallel to the  $ab$ -plane. Fig. 1c displays a typical device with a Hall bar geometry. The device is made by attaching the Fe<sub>3</sub>GaTe<sub>2</sub> thin flake on a pre-prepared Ti/Au electrode and covered by h-BN for protection from H<sub>2</sub>O and O<sub>2</sub>. The thickness  $t$  of this simple determined by the atomic force microscopy (AFM) (Fig. 1d) is around 12 nm. As shown in Fig. 1e, Fe<sub>3</sub>GaTe<sub>2</sub> with  $t = 12$  nm shows a metallic behavior in the range of 18 K - 320 K, and there is Kondo-like minimum at  $\sim 18$  K, similar to the results of Fe<sub>3</sub>GaTe<sub>2</sub> thin flakes in the literature.<sup>4</sup> Fig. 1f exhibits the field dependence of Hall resistivity  $\rho_{yx}(H)$  at 300 K with current  $I = +0.01$  mA and -0.01 mA applied along the  $ab$ -plane. The obvious hysteresis loop in the  $\rho_{yx}(H)$  curves clearly indicates that the room-temperature  $c$ -axial hard ferromagnetism persists in the Fe<sub>3</sub>GaTe<sub>2</sub> thin flake. Moreover, it can be seen that with small  $I$  ( $= \pm 0.01$  mA), the  $\rho_{yx}(H)$  curves with opposite current directions are almost same shape and both of them have identical  $H_c$  ( $\sim 70$  Oe).

Fe<sub>3</sub>GaTe<sub>2</sub> thin flakes exhibit an obvious behavior of current-dependent  $H_c$ . Taking the device with  $t = 12$  nm (sample 1, S1) as an example (Fig. 2a), at  $T = 5$  K, the hysteresis loop becomes smaller with the decreased  $H_c$  when the  $I$  increases. The  $H_c$  is around 2.5 kOe under  $I = 0.01$  mA and decrease to 1.8 kOe when a the 9 mA current is applied (Fig. 2b). In contrast to the significant changes of  $H_c$ , the saturation Hall resistivity  $\rho_{yx}^s$  related to the saturation magnetization is almost intact. Importantly, as shown in Figs. 2c and 2d, the current-controlled  $H_c$  still exists at room temperature ( $T = 300$  K). For  $I = 0.01$  mA, the  $H_c$  is  $\sim 70$  Oe and with increasing current the  $H_c$  decreases gradually. Finally it becomes almost

zero at  $I = 3$  mA. On the other hand, the  $\rho_{yx}^s$  is barely changed with current, similar to the results at 5 K. It implies that the ferromagnetic order is not been affected by the in-plane current and thus  $\text{Fe}_3\text{GaTe}_2$  is suitable for spintronics at room temperature. Fig. 2e displays the evolution of reduced  $H_c(I)/H_c(I = 0.01\text{mA})$  vs.  $I$  at different temperatures. The curves at the low-temperature region ( $T = 5 - 200$  K) exhibit similar behavior while the  $H_c$  decreases with increasing current more quickly at 250 K and 300 K. The larger current tunability of  $H_c$  at both temperatures can be partially ascribed to the weakened ferromagnetism because of the stronger thermal fluctuations at higher temperature. To confirm the reproducibility of properties of our devices, we measured several samples with different thicknesses (S1 - S3). They exhibit a similar reduction of  $H_c$  via  $I$  and the  $H_c$  of thinner sample decreases with  $I$  more quickly (Fig. S1 in Supporting Information). Fig. 2f shows the relationship between reduced  $H_c(J)/H_c(J \sim 0.01\text{mA}/\mu\text{m}^2)$  and current density at 300 K. It can be seen that all of curves for three devices almost fall on the same line, and the current reduces  $H_c$  by  $\sim 50$  % for  $\sim 5$  mA/ $\mu\text{m}^2$  when the  $H_c$  disappears at around  $J = 12.5$  mA/ $\mu\text{m}^2$ .

Based on the current-controlled coercivity reduction, we demonstrate that a highly energy-efficient nonvolatile spin memory device can be realized in  $\text{Fe}_3\text{GaTe}_2$  thin flakes at room temperature, in which magnetic information is written by  $I$  and read through the  $\rho_{yx}$ . Fig. 3a shows the hysteresis loop of  $\rho_{yx}(H)$  under 0.01 mA and 9 mA at 5 K. The negative and positive saturated magnetization states  $\pm M_s$  are defined as “0” and “1” states. When sweeping the field from -5 kOe to 2.2 kOe, the initial state of device is on the “0” state. Then a large writing current  $I_{\text{write}}$  of 9 mA is applied and because the  $H_c$  is significantly reduced by  $I_{\text{write}}$ , the magnetization of the  $\text{Fe}_3\text{GaTe}_2$  device can be switched by current from “0” state to “1” state (blue arrow). Correspondingly, the “1” state at -2.2 kOe initially can also be altered to “0” state by the large  $I_{\text{write}}$  (9 mA) (red arrow). Fig. 3b shows the detailed switching process of states through the  $\rho_{yx}(H) - \rho_{yx}(-5 \text{ kOe})$  as a function of  $I_{\text{write}}$  path (0  $\rightarrow$  9  $\rightarrow$  -9  $\rightarrow$  9 mA) under various fields from -5 kOe to 5 kOe. For the “0” state at  $H = -5$

kOe and the "1" state at  $H = 5$  kOe in  $\text{Fe}_3\text{GaTe}_2$  device, they are stable regardless of current sweep (purple and green curves). When fixing the field at 2.2 kOe, the increase of  $I_{\text{write}}$  from 0 to 9 mA leads to the change of magnetization gradually from  $-M_s$  ("0" state) to  $+M_s$  ("1" state). Importantly, after reaching the "1" state, the magnetization is unchanged even the  $I_{\text{write}}$  sweeps back to -9 mA and forth 9 mA again. It is clearly indicate that the magnetic information switching from "0" to "1" states through  $I_{\text{write}}$  is robust and nonvolatile (blue curve). Similarly, the reverse switching from "1" to "0" states can also be realized using the same  $I_{\text{write}}$  path with the field at -2.2 kOe (red curve). On the other hand, the magnetic information (the value of  $\rho_{yx}(H)$ ) can be read using a small current without disturbing the magnetization status. Similar results are also observed when  $H = \pm 1.8$  kOe and  $\pm 2.0$  kOe (Fig. S2 in Supporting Information), indicating that there is a relatively wide window of magnetic field to switch the "0" and "1" states by current. More importantly, such switching of magnetic states driven by current persists up to room temperature ( $T = 300$  K) (Figs. 3c and 3d). As shown in Fig. 3d, the "0" state at  $H = -1$  kOe and the "1" state at  $H = 1$  kOe are robust to the switching process  $I_{\text{write}}$  ( $0 \rightarrow 3 \rightarrow -3 \rightarrow 3$  mA) (purple and green curves). When fixing the field at  $\pm 20$  Oe, the increase of  $I_{\text{write}}$  from 0 to 3 mA can switch the magnetization gradually, similar to the case at 5 K. In addition, the minimum  $I_{\text{write}}$  ( $\sim 1$  mA) changing the "0" and "1" states at 300 K is much smaller than that at 5 K ( $\sim 6$  mA). Meanwhile, the field where the current can switch magnetic states also becomes very low (below 100 Oe). These behaviors are consistent with the significant reduction of  $H_c$  with  $I$  at 300 K (Fig. 2e). It is noted that at 300 K the hysteresis loop of  $\rho_{yx}(H)$  curve at 0.01 mA is not a rectangular shape and it disappears at 3 mA, thus the initial and final states at  $\pm 20$  Oe is slightly different from the "0" and "1" states at  $\pm 1$  kOe (green arrows in Figs. 3c and 3d). But the switching between the initial and final states at  $\pm 20$  Oe is still large enough to be discerned.

Next, we try to explain the electrical modulation of  $H_c$  qualitatively based on the SOT effect

generated by an in-plane current in Fe<sub>3</sub>GaTe<sub>2</sub> itself due to its special geometrical structure same as Fe<sub>3</sub>GeTe<sub>2</sub>.<sup>4</sup> Previous studies on Fe<sub>3</sub>GeTe<sub>2</sub> indicate that an in-plane current density  $\mathbf{J} = (J_x, J_y, 0)$  can induce a SOT  $\mathbf{T}_{\text{SOT}} = -|\gamma|\mathbf{M} \times \mathbf{H}_{\text{SOT}}$  acting on  $\mathbf{M} = (M_x, M_y, M_z)$ , where  $|\gamma|$  is the gyromagnetic ratio and the  $\mathbf{H}_{\text{SOT}}$  is the effective SOT magnetic field.<sup>17,23</sup> And the symmetry of the crystal determines the dependence of  $\mathbf{H}_{\text{SOT}}$  on  $\mathbf{m}$  and  $\mathbf{J}$  and it can be expressed as  $\mathbf{H}_{\text{SOT}} = \Gamma_0[(m_x J_x - m_y J_y)\mathbf{e}_x - (m_y J_x + m_x J_y)\mathbf{e}_y]$ , where  $\mathbf{m} = (m_x, m_y, m_z) = \mathbf{M}/|\mathbf{M}|$  is the magnetization unit vector and  $\Gamma_0$  is the strength of the magnetoelectric coupling, determined by the spin-orbital coupling.<sup>17,23</sup> Moreover, the  $\mathbf{H}_{\text{SOT}}$  can be obtained from an effective free energy density  $f_{\text{SOT}}$  by  $\mathbf{H}_{\text{SOT}} = -\partial f_{\text{SOT}}/\partial \mathbf{M}$  with  $f_{\text{SOT}} = M_s \Gamma_0 [J_y m_x m_y - \frac{1}{2} J_x (m_x^2 - m_y^2)]$ . Combined with the magnetocrystalline anisotropy energy (MAE) for Ising-type out-of-plane easy-axis ferromagnet  $f_{\text{MAE}} = -\frac{1}{2} K_z M_z^2 / M_s$ , we have the zero-field effective free energy density  $f_{\text{eff}} = f_{\text{MAE}} + f_{\text{SOT}}$ . If considering a spatially uniform magnetization and use a spherical basis,  $(m_x, m_y, m_z) = (\sin\theta\cos\phi, \sin\theta\sin\phi, \cos\theta)$  and  $(J_x, J_y, J_z) = |J|(\cos\phi_J, \sin\phi_J, 0)$ , it has  $f_{\text{eff}} = -\frac{1}{2} M_s [K_z \cos^2\theta + \Gamma_0 J \sin^2\theta \cos(2\phi + \phi_J)]$ .<sup>17,23</sup> For  $J = 0$ , the  $f_{\text{eff}}$  has a minimum value of  $-M_s K_z / 2$  at  $\mathbf{m} = \pm \mathbf{e}_z$  and a maximum value of 0 when  $\mathbf{m}$  lies in the  $xy$  plane. Therefore, the free energy barrier for switching the magnetization from  $\mathbf{m} = -\mathbf{e}_z$  to  $\mathbf{m} = +\mathbf{e}_z$  is  $M_s K_z / 2$ . In contrast, the existence of in-plane  $J$  modifies this free energy barrier to  $M_s (K_z - |\Gamma_0 J|) / 2$ , i.e., the  $J$  effectively reduce the barrier height between the local minima of the free energy.<sup>17</sup> Correspondingly, the coercive field  $H_c$  is also reduced from  $K_z$  at  $J = 0$  to  $K_z - |\Gamma_0 J|$  at finite in-plane  $J$  in a single domain case. This linear behavior is clearly observed from the  $H_c(J)$  curves for S1 - S3 of Fe<sub>3</sub>GaTe<sub>2</sub> at 300 K (Fig. 4a). The linear fits of  $H_c(J)$  curves at the low current density range give  $|\Gamma_0| = 7.0(3)$ ,  $5.7(3)$ , and  $8.4(5)$  Oe/(mA/ $\mu\text{m}^2$ ), respectively. These  $|\Gamma_0|$  values are comparable with Fe<sub>3</sub>GeTe<sub>2</sub>/Pt bilayer system,<sup>24</sup> and one order of magnitude larger than those in the conventional heavy metal multilayer films, such as Pt/Co and Pt/Fe etc<sup>17,24-28</sup> (Fig. 4(b)). Moreover, although the  $|\Gamma_0|$  of Fe<sub>3</sub>GaTe<sub>2</sub> in present work is somewhat smaller than that of Fe<sub>3</sub>GeTe<sub>2</sub> device,<sup>17</sup> the work temperature of Fe<sub>3</sub>GaTe<sub>2</sub> device at 300 K make it significantly

superior to  $\text{Fe}_3\text{GeTe}_2$ . On the other hand, lowering switching current density  $J_{\text{SW}}$  and power dissipation  $J_{\text{SW}}^2/\sigma$  ( $\sigma = 1/\rho$  is conductivity) are important to improve the energy efficiency of memory device. These two parameters of three  $\text{Fe}_3\text{GaTe}_2$  device have been calculated and shown in Fig. 4c. At 300 K, the  $J_{\text{SW}}$  and  $J_{\text{SW}}^2/\sigma$  are in the range of  $4.7(1)\text{-}7.7(3)\times 10^5$  A/cm<sup>2</sup> and  $1.5(0)\text{-}2.0(0)\times 10^{13}$  W/m<sup>3</sup>, both of which are significantly smaller than most of composite SOT systems. For example, the  $J_{\text{SW}}$  and  $J_{\text{SW}}^2/\sigma$  of  $\text{Fe}_3\text{GaTe}_2$  are about 300 and 60000 times smaller than conventional heavy-metal/magnet SOT Pt/Co system.<sup>27</sup> In addition, when compared with  $\text{Fe}_3\text{GeTe}_2$ , both of them have similarly small  $J_{\text{SW}}$  but the  $J_{\text{SW}}^2/\sigma$  of  $\text{Fe}_3\text{GaTe}_2$  is one order of magnitude lower than that of  $\text{Fe}_3\text{GeTe}_2$ , highlighting the high energy efficiency of present  $\text{Fe}_3\text{GaTe}_2$  devices.

In summary, the electrical control of coercive field in  $\text{Fe}_3\text{GaTe}_2$  thin flake devices is observed up to room temperature. In addition, the room-temperature nonvolatile magnetization switching behavior at very low field ( $\sim 20$  Oe) with a small in-plane current density ( $\sim 5.0\times 10^5$  A/cm<sup>2</sup>) and the remarkably low power dissipation ( $\sim 1.50 \times 10^{13}$  W m<sup>-3</sup>) is realized. These behaviors can be partially ascribed to the unique SOT effect in  $\text{Fe}_3\text{GaTe}_2$ . Such capability of high-efficiency nonvolatile magnetization switching by current at room temperature make  $\text{Fe}_3\text{GaTe}_2$  become a very promising system for spintronic applications using 2D magnetic vdW materials.

## Methods

**Single crystal growth and structural characterization.** Single crystals of  $\text{Fe}_3\text{GaTe}_2$  were grown by self-flux method. Flakes of Fe (99.98 % purity), Ga (99.99 % purity) and Te (99.99 %) in a molar ratio of 1 : 1 : 2 were put into a quartz tube. The tube was evacuated and sealed at 0.01 Pa. The sealed quartz ampoule was heated to 1273 K for 10 hours and are then held there for another one day, then held there for another one day, then the temperature was quickly decrease down to 1153 K within 2 h followed by slowly

cooled down to 1053 K within 100 h. Finally, the ampoule was taken out from the furnace and decanted with a centrifuge to separate  $\text{Fe}_3\text{GaTe}_2$  single crystals from the flux. In order to avoid degradation, the  $\text{Fe}_3\text{GaTe}_2$  single crystals are stored in an Ar-filled glovebox. The XRD pattern of a  $\text{Fe}_3\text{GaTe}_2$  single crystal was measured using a Bruker D8 Advance X-ray machine with  $\text{Cu K}\alpha$  ( $\lambda = 1.5418 \text{ \AA}$ ) radiation. For the fit of lattice parameters of  $\text{Fe}_3\text{GaTe}_2$ , the single-crystal XRD pattern was measured using a Bruker D8 Quest X-ray machine with  $\text{Mo K}\alpha$  ( $\lambda = 0.7107 \text{ \AA}$ ) radiation. The microscopy images was acquired using a Bruker Edge Dimension atomic force microscope (AFM).

**Device fabrication.**  $\text{Fe}_3\text{GaTe}_2$  flakes were cleaved from bulk crystals onto polydimethylsiloxane (PDMS) by mechanical exfoliation and they were examined by an optical microscope to evaluate the thickness roughly. Then the atomically smooth flakes with desired thicknesses were transferred to a 285 nm  $\text{SiO}_2/\text{Si}$  substrate with pre-patterned electrodes and an  $h$ -BN capping layer was used to cover the sample for protection from  $\text{H}_2\text{O}$  and  $\text{O}_2$ . The Ti/Au (10/40 nm) electrodes was fabricated by electron beam lithography and metals were deposited using thermally evaporating method. After transport measurements, the  $h$ -BN capping layer was removed and the thickness of sample was determined precisely by AFM. The whole fabrication process of device was carried out in an argon glove box with  $\text{H}_2\text{O}$  and  $\text{O}_2$  contents less than 0.1 ppm to avoid degradation of the samples.

**Electrical transport measurements.** Magnetization and electrical transport measurements were performed in a Quantum Design MPMS3 and superconducting magnet system (Cryomagnetics, C-Mag Vari-9). Both longitudinal and Hall electrical resistance were measured using a five-probe method on  $\text{Fe}_3\text{GaTe}_2$  Hall bar device with current flowing in the  $ab$  plane. In dc measurements, the bias current was generated by using a current source (Keithley, 6221) and the voltage was measured with a nanovoltmeter (Keithley, 2182A). The raw Hall resistance was measured by sweeping the field up to  $\pm 5$  kOe at various temperatures, and the Hall resistance was determined by a standard symmetrization procedure to remove the contribution of magnetoresistance from the raw Hall data due to voltage probe

misalignment.<sup>30</sup>

## Supporting Information Available

Figure S1. The  $H_c(I)/H_c(I = 0.01\text{mA})$  as a function of current  $I$  for three devices at 300 K;  
Figure S2. Nonvolatile magnetization switching by current under fields  $\pm 1.8$  kOe and  $\pm 2.0$  kOe at 5 K.

## Acknowledgement

This work was supported by National Key R&D Program of China (Grants Nos. 2018YFE0202600 and 2022YFA1403800), Beijing Natural Science This work was supported by National Key R&D Program of China (Grants Nos. 2018YFE0202600 and 2022YFA1403800), Beijing Natural Science Foundation (Grant No. Z200005), National Natural Science Foundation of China (Grants No. 12174443), the Fundamental Research Funds for the Central Universities and Research Funds of Renmin University of China (RUC) (Grants Nos. 18XNLG14 and 19XNLG17), the Outstanding Innovative Talents Cultivation Funded Programs 2022 of Renmin University of China, Beijing National Laboratory for Condensed Matter Physics, and Collaborative Research Project of Laboratory for Materials and Structures, Institute of Innovative Research, Tokyo Institute of Technology.

## References

- (1) Gong, C.; Li, L.; Li, Z.; Ji, H.; Stern, A.; Xia, Y.; Cao, T.; Bao, W.; Wang, C.; Wang, Y.; Qiu, Z. Q.; Cava, R. J.; Louie, S. G.; Xia, J.; Zhang, X. Discovery of intrinsic ferromagnetism in two-dimensional van der Waals crystals. *Nature* **2017**, 546, 265-269.
- (2) Huang, B.; Clark, G.; Navarro-Moratalla, E.; Klein, D. R.; Cheng, R.; Seyler, K. L.; Zhong, D.; Schmidgall, E.; McGuire, M. A.; Cobden, D. H.; Yao, W.; Xiao, D.; Jarillo-

- Herrero, P.; Xu, X. Layer-dependent ferromagnetism in a van der Waals crystal down to the monolayer limit. *Nature* **2017**, 546, 270-273.
- (3) Deng, Y.; Yu, Y.; Song, Y.; Zhang, J.; Wang, N. Z.; Sun, Z.; Yi, Y.; Wu, Y. Z.; Wu, S.; Zhu, J.; Wang, J.; Chen, X. H.; Zhang, Y. Gate-tunable room-temperature ferromagnetism in two-dimensional  $\text{Fe}_3\text{GeTe}_2$ . *Nature* **2018**, 563, 94-99.
- (4) Zhang, G.; Guo, F.; Wu, H.; Wen, X.; Yang, L.; Jin, W.; Zhang, W.; Chang, H. Above-room-temperature strong intrinsic ferromagnetism in 2D van der Waals  $\text{Fe}_3\text{GaTe}_2$  with large perpendicular magnetic anisotropy. *Nat. Commun.* **2022**, 13, 5067.
- (5) Tian, S.; Zhang, J.-F.; Li, C.; Ying, T.; Li, S.; Zhang, X.; Liu, K.; Lei, H. Ferromagnetic van der Waals Crystal  $\text{VI}_3$ . *J. Am. Chem. Soc.* **2019**, 141, 5326-5333.
- (6) Lee, J.-U.; Lee, S.; Ryoo, J. H.; Kang, S.; Kim, T. Y.; Kim, P.; Park, C.-H.; Park, J.-G.; Cheong, H. Ising-Type Magnetic Ordering in Atomically Thin  $\text{FePS}_3$ . *Nano Lett.* **2016**, 16, 7433-7438.
- (7) Lee, K.; Dismukes, A. H.; Telford, E. J.; Wiscons, R. A.; Wang, J.; Xu, X.; Nuckolls, C.; Dean, C. R.; Roy, X.; Zhu, X. Magnetic Order and Symmetry in the 2D Semiconductor  $\text{CrSBr}$ . *Nano Lett.* **2021**, 21, 3511-3517.
- (8) Geim, A. K.; Grigorieva, I. V. Van der Waals heterostructures. *Nature* **2013**, 499, 419-425.
- (9) Novoselov, K. S.; Mishchenko, A.; Carvalho, A.; CastroNeto, A. H. 2D materials and van der Waals heterostructures. *Science* **2016**, 353, aac9439.
- (10) Liu, Y.; Weiss, N. O.; Duan, X.; Cheng, H.-C.; Huang, Y.; Duan, X. Van der Waals heterostructures and devices. *Nat. Rev. Mater.* **2016**, 1, 16042.
- (11) Deiseroth, H.-J.; Aleksandrov, K.; Reiner, C.; Kienle, L.; Kremer, R. K.  $\text{Fe}_3\text{GeTe}_2$  and  $\text{Ni}_3\text{GeTe}_2$  - Two new layered transition-metal compounds: Crystal structures, HRTEM

- investigations, and magnetic and electrical properties. *Eur. J. Inorg. Chem.* **2006**, 8, 1561.
- (12) May, A. F.; Ovchinnikov, D.; Zheng, Q.; Hermann, R.; Calder, S.; Huang, B.; Fei, Z.; Liu, Y.; Xu, X.; McGuire, M. A. Ferromagnetism Near Room Temperature in the Cleavable van der Waals Crystal  $\text{Fe}_5\text{GeTe}_2$ . *ACS Nano* **2019**, 13, 4436-4442.
- (13) Seo, J.; Kim, D. Y.; An, E. S.; Kim, K.; Kim, G.-Y.; Hwang, S.-Y.; Kim, D. W.; Jang, B. G.; Kim, H.; Eom, G.; et al. Nearly room temperature ferromagnetism in a magnetic metal-rich van der Waals metal. *Sci. Adv.* **2020**, 6, eaay8912.
- (14) Li, Z.; Tang, M.; Huang, J.; Qin, F.; Ao, L.; Shen, Z.; Zhang, C.; Chen, P.; Bi, X.; Qiu, C.; Yu, Z.; Zhai, K.; Ideue, T.; Wang, L.; Liu, Z.; Tian, Y.; Iwasa, Y.; Yuan, H. Magnetic Anisotropy Control with Curie Temperature above 400 K in a van der Waals Ferromagnet for Spintronic Device. *Adv. Mater.* **2022**, 34, 2201209.
- (15) Eyers, E. B.; Ralph, D. C.; Katine, J. A.; Louie, R. N.; Buhrman, R. A. Current-induced switching of domains in magnetic multilayer devices. *Science* **1999**, 285, 867.
- (16) Wang, Q. Y.; Zeng, Y.; Yuan, K.; Zeng, Q. Q.; Gu, P. F.; Xu, X. L.; Wang, H. W.; Han, Z.; Nomura, K.; Wang, W. H.; Liu, E. K.; Hou, Y. L.; Ye, Y. Magnetism modulation in  $\text{Co}_3\text{Sn}_2\text{S}_2$  by current-assisted domain wall motion. *Nat. Electron.* **2022**, 6, 119.
- (17) Zhang, K.; Han, S.; Lee, Y.; Coak, M. J.; Kim, J.; Hwang, I.; Son, S.; Shin, J.; Lim, M.; Jo, D.; Kim, K.; Kim, D.; Lee, H.-W.; Park, J.-G. Gigantic Current Control of Coercive Field and Magnetic Memory Based on Nanometer-Thin Ferromagnetic van der Waals  $\text{Fe}_3\text{GeTe}_2$ . *Adv. Mater.* **2021**, 33, 2004110.
- (18) Zhang, K.; Lee, Y.; Coak, M. J.; Kim, J.; Son, S.; Hwang, I.; Ko, D.-S.; Oh, Y.; Jeon, I.; Kim, D.; Zeng, C.; Lee, H.-W.; Park, J.-G. Highly Efficient Nonvolatile Magnetization Switching and Multi-Level States by Current in Single Van der Waals Topological Ferromagnet  $\text{Fe}_3\text{GeTe}_2$ . *Adv. Funct. Mater.* **2021**, 31, 2105992.

- (19) Zhu, W. K.; Xie, S. H.; Lin, H. L.; Zhang, G. J.; Wu, H.; Hu, T. G.; Wang, Z.; Zhang, X. M.; Xu, J. H.; Wang, Y. J.; Zheng, Y. H.; Yan, F. G.; Zhang, J.; Zhao, L. X.; Patane, A.; Zhang, J.; Chang, H. X.; Wang, K. Y. Large room-temperature magnetoresistance in van der Waals ferromagnet/semiconductor junctions. *Chin. Phys. Lett.* **2022**, *39*, 128501.
- (20) Yin, H.; Zhang, P.; Jin, W.; Di, B.; Wu, H.; Zhang, G.; Zhang, W.; Chang, H. Fe<sub>3</sub>GaTe<sub>2</sub>/MoSe<sub>2</sub> Ferromagnet/Semiconductor 2D van der Waals Heterojunction for Room-Temperature Spin-Valve Devices. *CrystEngComm*, **2023**, *25*, 1339-1346.
- (21) Jin, W.; Zhang, G.; Wu, H.; Yang, L.; Zhang, W.; Chang, H. Room-Temperature Spin-Valve Devices Based on Fe<sub>3</sub>GaTe<sub>2</sub>/MoSe<sub>2</sub>/Fe<sub>3</sub>GaTe<sub>2</sub> 2D van der Waals Heterojunctions. *Nanoscale*, **2023**, *15*, 5371-5378.
- (22) Li, W.; Zhu, W.; Zhang, G.; Wu, H.; Zhu, S.; Li, R.; Zhang, E.; Zhang, X.; Deng, Y.; Zhang, J.; Zhao, L.; Chang, H.; Wang, K. Room-temperature van der Waals 2D ferromagnet switching by spin-orbit torques. **2023**, *arXiv: 2304.10718*
- (23) Johansen, O.; Risinggard, V.; Sudbo, A.; Linder, J.; Brataas, A. Current Control of Magnetism in Two-Dimensional Fe<sub>3</sub>GeTe<sub>2</sub>. *Phys. Rev. Lett.* **2019**, *122*, 217203.
- (24) Wang, X.; Tang, J.; Xia, X.; He, C.; Zhang, J.; Liu, Y.; Wan, C.; Fang, C.; Guo, C.; Yang, W.; et al. Current-driven magnetization switching in a van der Waals ferromagnet Fe<sub>3</sub>GeTe<sub>2</sub>. *Sci. Adv.* **2019**, *5*, eaaw8904.
- (25) Khang, N. H. D.; Ueda, Y.; Hai, P. N. A conductive topological insulator with large spin Hall effect for ultra low power spin-orbit torque switching. *Nat. Mater.* **2018**, *17*, 808-813.
- (26) Han, J.; Richardella, A.; Siddiqui, S. A.; Finley, J.; Samarth, N.; Liu, L. Room-Temperature Spin-Orbit Torque Switching Induced by a Topological Insulator. *Phys. Rev. Lett.* **2017**, *119*, 077702.

- (27) Garello, K.; Miron, I. M.; Avci, C. O.; Freimuth, F.; Mokrousov, Y.; Blugel, S.; Auffret, S.; Boulle, O.; Gaudin, G.; Gambardella, P. Symmetry and magnitude of spin-orbit torques in ferromagnetic heterostructures. *Nat. Nanotechnol.* **2013**, 8, 587.
- (28) DC, M.; Grassi, R.; Chen, J.-Y.; Jamali, M.; Hickey, D. R.; Zhang, D.; Zhao, Z.; Li, H.; Quarterman, P.; Lv, Y.; Li, M.; Manchon, A.; Mkhoyan, K. A.; Low, T.; Wang, J.-P. Room-temperature high spin-orbit torque due to quantum confinement in sputtered  $\text{Bi}_x\text{Se}_{(1-x)}$  films. *Nat. Mater.* **2018**, 17, 800-807.
- (29) Wang, Y.; Zhu, D.; Wu, Y.; Yang, Y.; Yu, J.; Ramaswamy, R.; Mishra, R.; Shi, S.; Elyasi, M.; Teo, K.-L.; Wu, Y.; Yang, H. Room temperature magnetization switching in topological insulator-ferromagnet heterostructures by spin-orbit torques. *Nat. Commun.* **2017**, 8, 1364.
- (30) Ohno, H.; Munekata, H.; Penny, T.; Molnar, S. V.; Chang, L. L. Magnetotransport properties of p-type (In,Mn)As diluted magnetic III-V semiconductors. *Phys. Rev. Lett.* **1992**, 68, 2664.

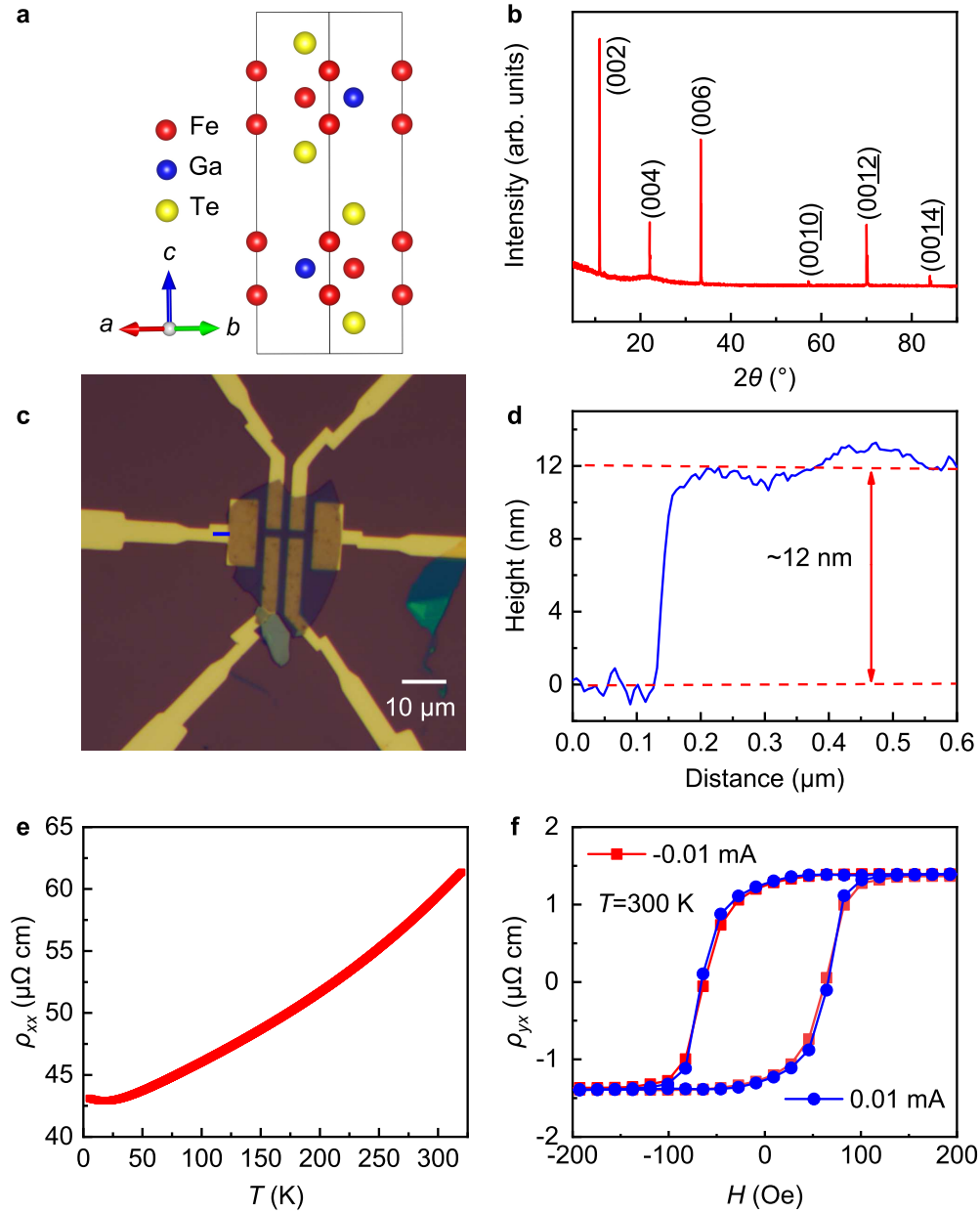


Figure 1: **Crystal structure and transport properties of a typical  $\text{Fe}_3\text{GaTe}_2$  thin flake.** **a**, Crystal structure of  $\text{Fe}_3\text{GaTe}_2$ . The red, blue and yellow balls represent Fe, Ga and Te atoms, respectively. **b**, XRD pattern of a  $\text{Fe}_3\text{GaTe}_2$  single crystal. **c**, Optical image of a  $\text{Fe}_3\text{GaTe}_2$  thin flake on a 285 nm  $\text{SiO}_2/\text{Si}$  substrate. The white scale bar represents 10  $\mu\text{m}$ . **d**, Cross-sectional profile of the  $\text{Fe}_3\text{GaTe}_2$  thin flake along the blue line in **c**. **e**, Temperature dependence of  $\rho_{xx}(T)$  for  $\text{Fe}_3\text{GaTe}_2$  with  $t = 12$  nm. **f**, Field dependence of  $\rho_{yx}(H)$  at 300 K with  $ab$ -plane currents of +0.01 mA and -0.01 mA .

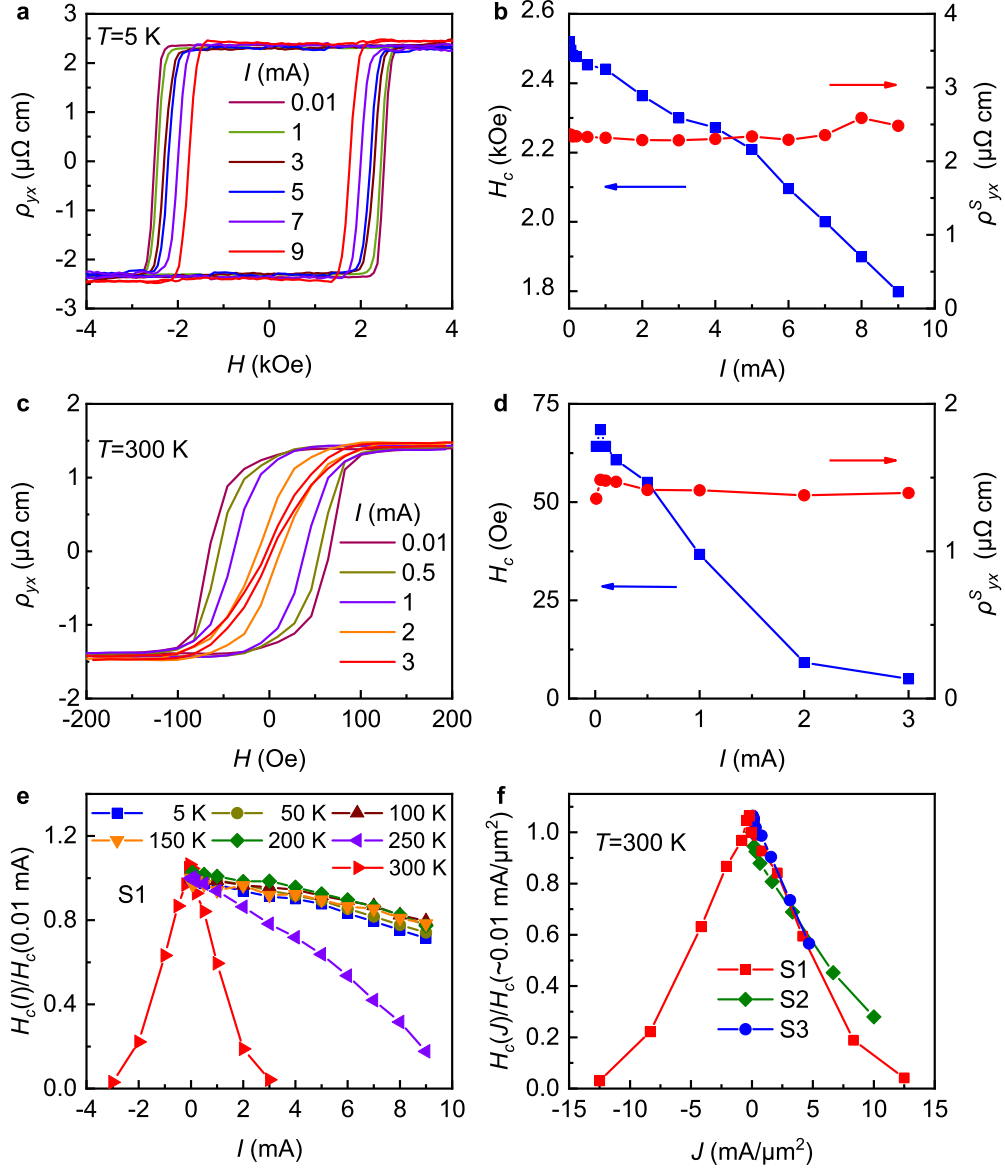


Figure 2: **Evolution of  $\rho_{yx}(H)$  hysteresis loop with  $I$  in  $\text{Fe}_3\text{GaTe}_2$  thin flakes.** **a**, Field dependence of  $\rho_{yx}(H)$  with an in-plane  $I$  from 0.01 mA to 9 mA for sample 1 (S1) at 5 K. **b**, the  $H_c$  and  $\rho_{yx}^s$  as a function of  $I$  for S1 at 5 K. **c**, Field dependence of  $\rho_{yx}(H)$  at various  $I$  at 300 K. **d**, the  $I$  dependence of  $H_c$  and  $\rho_{yx}^s$  for S1 at 300 K. **e**, the  $I$  dependence of  $H_c(I)/H_c(I = 0.01\text{mA})$  at different temperatures for S1. **f**, the  $H_c(J)/H_c(J = 0.01\text{mA}/\mu\text{m}^2)$  as a function of  $J$  for three devices at 300 K.

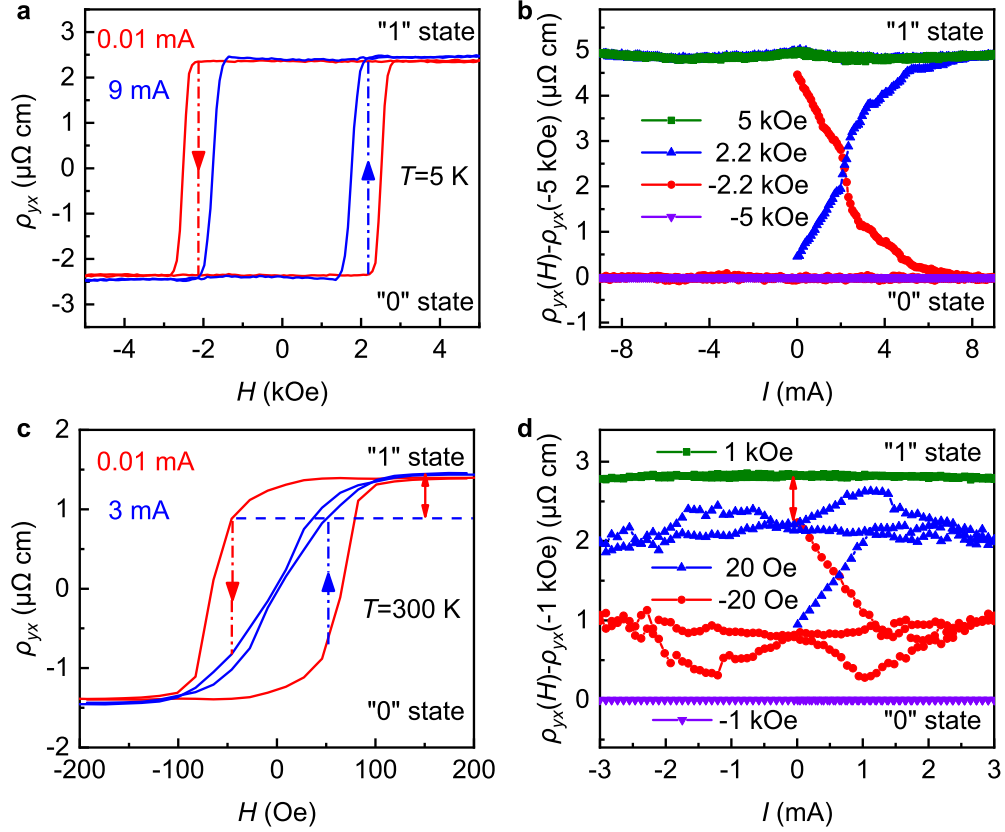


Figure 3: **Nonvolatile magnetization switching by current.** **a**,  $\rho_{yx}(H)$  curves of sample S1 under  $I = 0.01$  mA and 9 mA at  $T = 5$  K. The blue and red arrows indicate the transitions between “0” and “1” states driven by current at  $H = \pm 2.2$  kOe. **b**,  $\rho_{yx}(H) - \rho_{yx}(-5 \text{ kOe})$  as a function of writing current  $I_{\text{write}}$  path ( $0 \rightarrow 9 \rightarrow -9 \rightarrow 9$  mA) under various fields from -5 kOe to 5 kOe at 5 K. The red and blue curve shows the switching from “1” to “0” and “0” to “1”, respectively. **c**,  $\rho_{yx}(H)$  curves of sample S1 under  $I = 0.01$  mA and 3 mA at  $T = 300$  K. **d**,  $\rho_{yx}(H) - \rho_{yx}(-1 \text{ kOe})$  as a function of writing current  $I_{\text{write}}$  path ( $0 \rightarrow 3 \rightarrow -3 \rightarrow 3$  mA) under various fields from -1 kOe to 1 kOe at 300 K. The red and blue curve shows the switching from “1” to “0” and “0” to “1”, respectively.

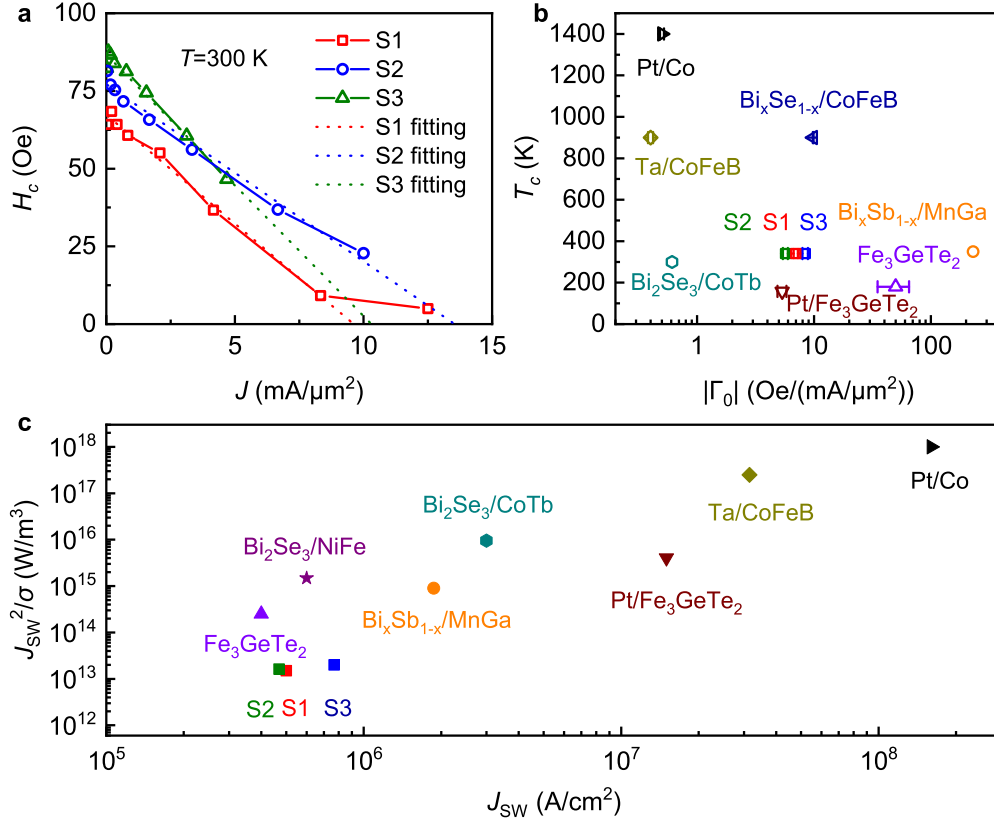


Figure 4: **Highly efficient magnetization switching by current at 300 K.** **a**,  $J$  dependence of  $H_c$  at 300 K and linear fits at low current density range for S1-S3. **b**,  $|\Gamma_0|$  and  $T_c$  of  $\text{Fe}_3\text{GaTe}_2$  and other SOT systems.<sup>17,24–28</sup> **c**, Switching current density  $J_{\text{sw}}$  and switching power dissipation  $J_{\text{sw}}^2/\sigma$  of  $\text{Fe}_3\text{GaTe}_2$  and various SOT systems.<sup>17,24–29</sup> The data for  $\text{Fe}_3\text{GaTe}_2$  and Pt/ $\text{Fe}_3\text{GaTe}_2$  is measured at 2 K and 140 K, respectively, when other data are obtained at 300 K.